Materials Sciences and Applications, 2012, 3, 355-362
http://dx.doi.org/10.4236/msa.2012.36051 Published Online June 2012 (http://www.SciRP.org/journal/msa)

Effect of Antimony Additions on Corrosion and Mechanical Properties of Sn-Bi Eutectic Lead-Free Solder Alloy

Alberto Torres, Luis Hernández, Octavio Domínguez*

Instituto de Metalurgia-UASLP, San Luis Potosí, México.
Email: *nanochemmex@yahoo.com

Received February 29th, 2012; revised March 28th, 2012; accepted April 27th, 2012

ABSTRACT

The goal of the present work is to investigate the effects of the addition of Sb (0, 3 and 6 wt%) on structure, melting, corrosion and mechanical properties of Sn-Bi eutectic solder alloys. The mechanical properties of the bulk Sn-Bi-Sb solders were higher as the amount of antimony increases, making compressive strength augment from 65 MPa to 100 MPa when 6 wt% Sb was incorporated to the Sn-Bi eutectic alloy. The three alloys presented a melting temperature that is smaller to the one exhibited by the eutectic alloy Sn-38Pb (T_m = 183˚C). According to the electrochemical results, the addition of higher contents of Sb to the Sn-Bi eutectic alloy had a positive effect: it ennobled the E_{corr} values.

Keywords: Lead Free Solder Alloys; Sn-Bi-Sb; Mechanical Properties; Corrosion Properties

1. Introduction

Due to the toxicity and harmful environmental effect of Pb present in tin solders, legislation trend to reduce or eliminate the utilization of lead from a wide variety of uses. There are many different metals and metal alloys that can be used as solders and a set of binary alloys have been chosen as candidates for lead-free solders: Sn-Bi, Sn-Ag, Sn-Zn, Sn-Cu and Sn-Sb. Among the ternary compositions, the Sn-Bi-Zn one was used in making printing wiring boards [1], however all of these eutectic compositions have a melting temperature above 200˚C. Sn-Zn eutectic has a lower melting temperature of 199˚C, but its corrosion behavior and poor wetting ability renders it useless [2]. Among the commercial Pb-free alloys, Sn-58 wt% Bi eutectic alloy may be a favorable alloy specially for electronics and telecommunications. In fact, this alloy, which has the eutectic temperature of 139˚C, has a higher ultimate tensile stress and shear strength than Sn-Pb eutectic [2,3]. Bismuth has also been used as the alloying element in ternary Sn-Zn-Bi [4] Sn-Ag-Bi [5,6] and Sn-Bi-Cu [7] systems to provide suitable substitutes for Sn-Pb solder alloys.

In an effort to develop lead-free solders, most research up to now focused on melting points and physical strengths of alloys, and there has been little consideration of the corrosion properties of base alloys for lead-free solders [8-10]. Moreover, the properties of these Sn-Bi-Sb lead-free alloys in corrosive environments have not been reported, and most of the fluxes are chloride or fluoride base compounds. As a result, most of the corrosion associated with soldered joints is due to the use of improper or insufficient cleaning methods to remove the fluxes [11]. Consequently, the objective of this preliminary study is to investigate the effects of the addition of Sb on structure, melting, corrosion and mechanical properties of Sn-Bi eutectic solder alloys.

2. Experimental Procedure

2.1. Materials and Processing

The materials used were three Sn-58% Bi alloys, containing 0, 3 and 6 wt% Sb. The samples were prepared from high purity (99.99%) tin, bismuth and antimony metals, melted in an electrical furnace under inert argon atmosphere and cast into slabs in alumina crucibles. The chemical composition of the produced alloys was determined by Atomic Absorption Spectrometry (**Table 1**).

Table 1. Chemical composition of manufactured alloys (wt%).

SYSTEM	*Nominal*	*Experimental*
Sn58Bi0Sb	58Bi-42Sn	57.45Bi-42.55Sn
Sn58Bi3Sb	56.25Bi-40.75Sn-3Sb	56.18Bi-40.77Sn-3.05Sb
SnBi-6Sb	54.52Bi-39.48Sn-6Sb	53.23Bi-41.02Sn-5.75Sb

*Corresponding author.

2.2. Thermal, Structural, Mechanical and Electrochemical Characterization

The thermal behavior of the alloys was investigated using a Perkin-Elmer differential scanning calorimeter (DSC). The specimens with an approximate weight of 50 mg were heated to 300˚C, under inert argon atmosphere, with a constant rate of 10˚C/min. The structure of the alloys was examined by X-ray diffraction (XRD) using a Rigaku diffractometer with CuK radiation (λ = 1.54056 A). A scanning electron microscope (SEM) model Philips XL-30 was used for microstructural analysis and energy dispersive X-ray spectroscopy (EDX) was performed in the SEM to analyze the chemical composition of the alloys. The compressive tests were conducted at room temperature using a Shimadzu AG-I universal testing machine with a constant cross-head speed of 0.5 mm/min. Vickers hardness (VH) was measured using a Vickers microhardness tester.

The specimens were polished with grade 600 and 1000 carborundum papers, rinsed with distilled water and acetone and dried with hot air, previously to the electrochemical tests. The open circuit corrosion potential (E_{corr}) of all specimens was recorded before the potentiodynamic polarization measurements using a saturated calomel electrode (SCE) as reference. It was used a cell for flat samples, with a contact area of 1 cm^2 between working electrode and electrolyte (a 3% NaCl solution). The cell contained a great superficial area platinum electrode as the counter electrode, and the reference electrode already mentioned. Potentiodynamic polarization measurements were conducted with a scan rate of 10 mV/min. Cathodic potentiodynamic scans were carried out first, starting at the E_{corr} value to around −1200 mV_{sce}. Anodic scans were done, after a return to steady-state conditions, from the E_{corr} value to around 500 mV_{sce}. All electrochemical measurements were carried out at room temperature and with no de-aeration of the electrolyte.

3. Results and Discussion

3.1. Phases and Microstructure

Figure 1 shows the corresponding Sn-Bi, Bi-Sb and Sn-Sb binary phase diagrams. The Sn-Bi system displays a eutectic reaction with 43 atomic% of bismuth (58 wt%) at a temperature of 139˚C. In contrast, the Bi-Sb system freeze to form a continuous series of solid solutions, contrary to the Sn-Sb system where the tin rich zone exhibits a peritectic reaction and limited solid solution of Sb.

Figure 2 shows the X-ray diffraction pattern of the as-cast Sn-58% Bi alloy showing the only presence of β-Sn and Bi, with no other compounds. SEM images of the as cast eutectic Sn-58 wt% Bi alloy, obtained under conventional cooling rates, produced a fine lamellar structure.

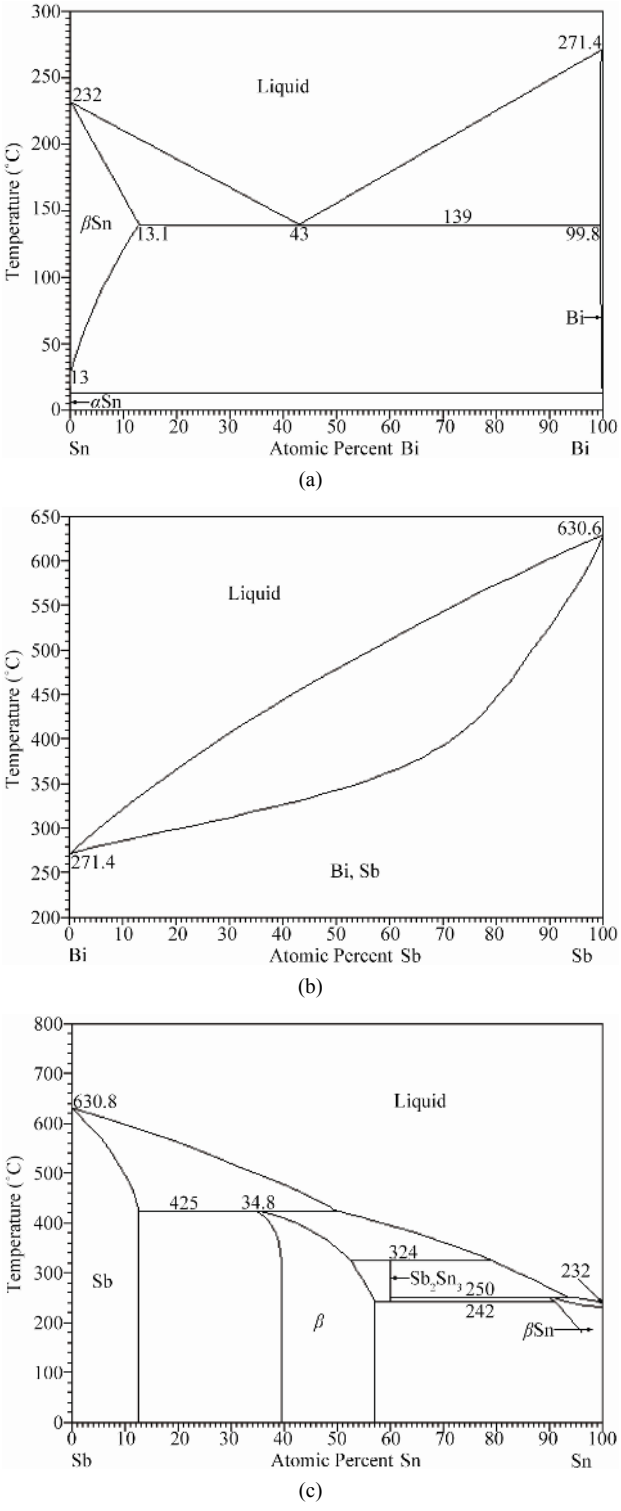

Figure 1. (a) Binary Sn-Bi phase diagram presenting the eutectic reaction; (b) Bi-Sb phase diagram exhibiting complete solid solubility; (c) Binary Sb-Sn phase diagram presenting the peritectic reaction [12].

Eutectic alloys composed of a metallic phase and a

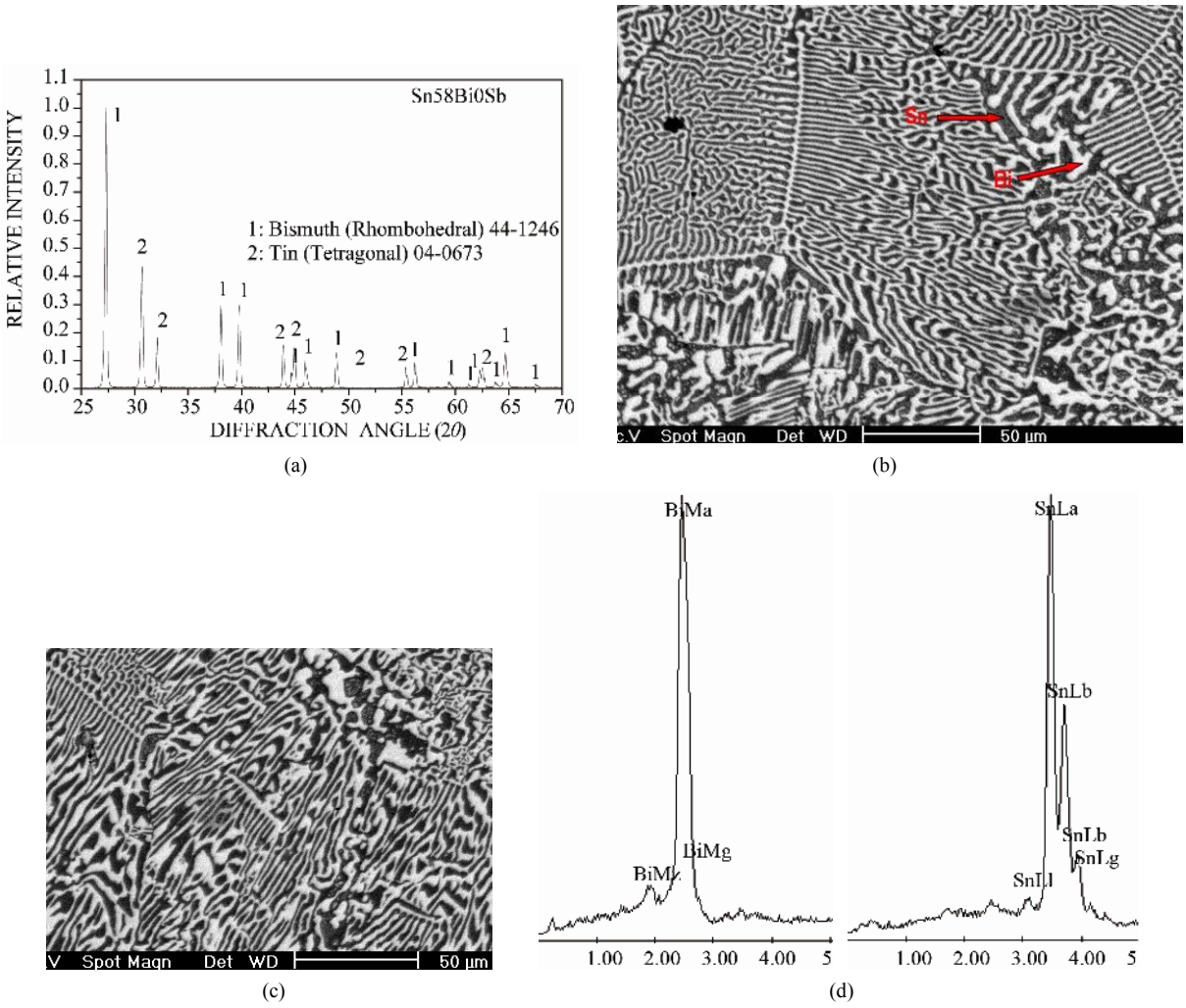

Figure 2. (a) XRD pattern obtained from the Sn-58% Bi alloy; (b) Low magnification image obtained by SEM; (c) High magnification image indicating an interface spacing of 2.5 µm; (d) EDX chemical analysis of the same alloy.

semiconductor phase generally have a type II (complex regular) or type III (irregular) structure [13,14]. In the complex regular microstructure one observes two types of regions, one zones of a repeating regular pattern and other zones of random orientation as those observed on **Figure 2(b)**. Besides, from image on **Figure 2(c)** obtained at higher magnification of the Sn-58 wt% Bi alloy, a mean interface spacing of 2.5 µm was measured. EDX analysis carried out on this sample indicated that the white planar phase was made of bismuth while the black phase corresponded to pure tin (**Figure 2(d)**), therefore corroborating the SEM images.

On the other hand, **Figure 3(a)** shows the X-ray diffraction pattern of the Sn-58 wt% Bi-3 wt% Sb alloy, indicating the presence of pure β-Sn, Bi and the occurrence of the intermetallic compound SbSn, in agreement to the Sb-Sn equilibrium diagram shown in **Figure 1(c)**. As before, SEM images of the solidified eutectic Sn-58 wt% Bi-3 wt% Sb alloy obtained with the same casting cooling rates are shown in **Figure 3**. In this case, the resulting microstructure slightly differs from the first one, resulting in smaller zones of lamellar structure together with random oriented regions and coarse globular β-Sn rich phase (**Figure 3(b)**). In the present case, at higher magnification a mean interface secondary eutectic spacing of 1.5 µm was measured in the lamellar regions (**Figure 3(c)**). EDX analysis carried out on sample Sn-58 wt% Bi-3 wt% Sb indicated once again that the white planar phase was only bismuth while the black zone corresponded to the β-Sn rich phase. From EDX analysis carried out on **Figure 3(d)** at high magnification in the globular phase with high content of β-Sn, it was not possible to detect the presence of Sb inside the sub-microstructure observed in these regions.

Augmenting the addition of antimony, **Figure 4** shows the X-ray diffraction pattern of the Sn-58 wt% Bi-6 wt% Sb alloy, indicating the presence of pure β-Sn, Bi and the intermetallic compound SbSn. SEM images of the solidi-

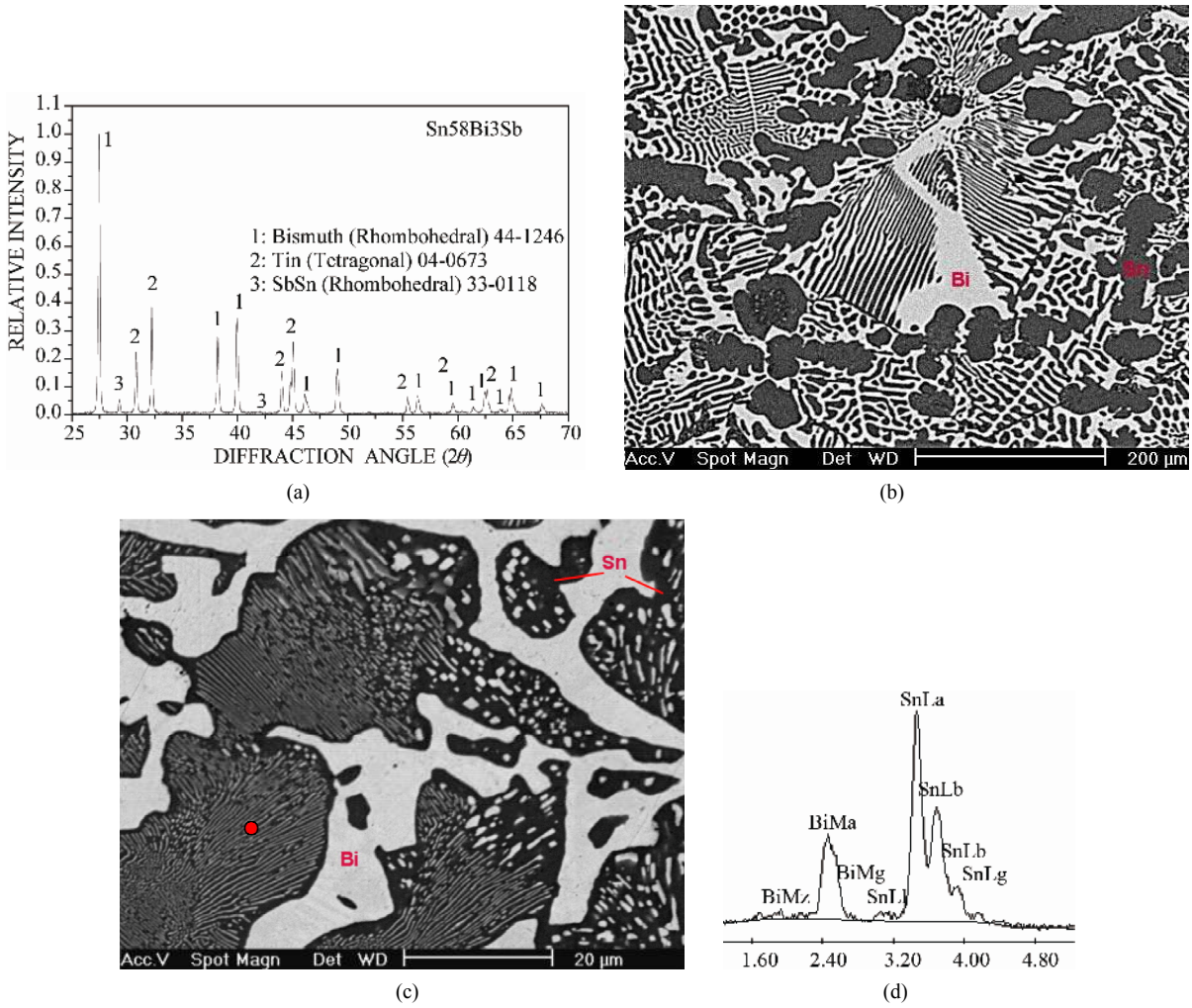

Figure 3. (a) XRD pattern obtained from the Sn-58% Bi-3% Sb alloy; (b) Low magnification image obtained by SEM from Sn-58% Bi-3% Sb alloy; (c) High magnification SEM image of the same alloy; (d) EDX chemical analysis of selected red zone.

fied eutectic Sn-58 wt% Bi-6 wt% Sb alloy processed in the same way as before, suggested that the resulting microstructure in this case was noticeably different from the other two alloys, resulting in random oriented regions and β-Sn rich dendritic phase (**Figures 4(b)** and **(c)**), so in the present case there are no eutectic lamellar regions. A planar eutectic solid/liquid interface can become unstable just as in the case of a single-phase interface. There are different ways in which instability can develop, and a reported trend corresponds to the presence of a third element that destabilizes the morphology as a whole because a long-range diffusion boundary is established ahead of the composite solid/liquid interface [15,16]. Therefore, the eutectic alloy composed with 6 wt% of Sb has almost changed to type III (irregular) structure. Hence, the higher concentration of the third element induces the instability of just one phase, leading to the appearance of dendrites in the solid/liquid interface.

EDX analysis carried out on sample Sn-58 wt% Bi-6 wt% Sb indicated once again that the white planar phase was only bismuth while the black zone corresponded to the β-Sn rich phase. From EDX analysis carried out on **Figure 4(d)** at elevated magnification, it was not possible to detect the presence of Sb inside the observed microstructure. Probably the reason why there is always a lack of signal associated to antimony could be associated to the EDX spectrometric technique. In general, the EDX energy resolution of the equipment is about 230 eV and the difference in L_α electron binding energy transition between Sn and Sb correspond to approximately 205 eV.

3.2. Thermal, Mechanical and Electrochemical Properties

Figure 5 shows the thermodiagrams obtained by DSC of the manufactured Sn-Bi-Sb alloys. It is important to note that the gap between T_s and T_L temperatures increases

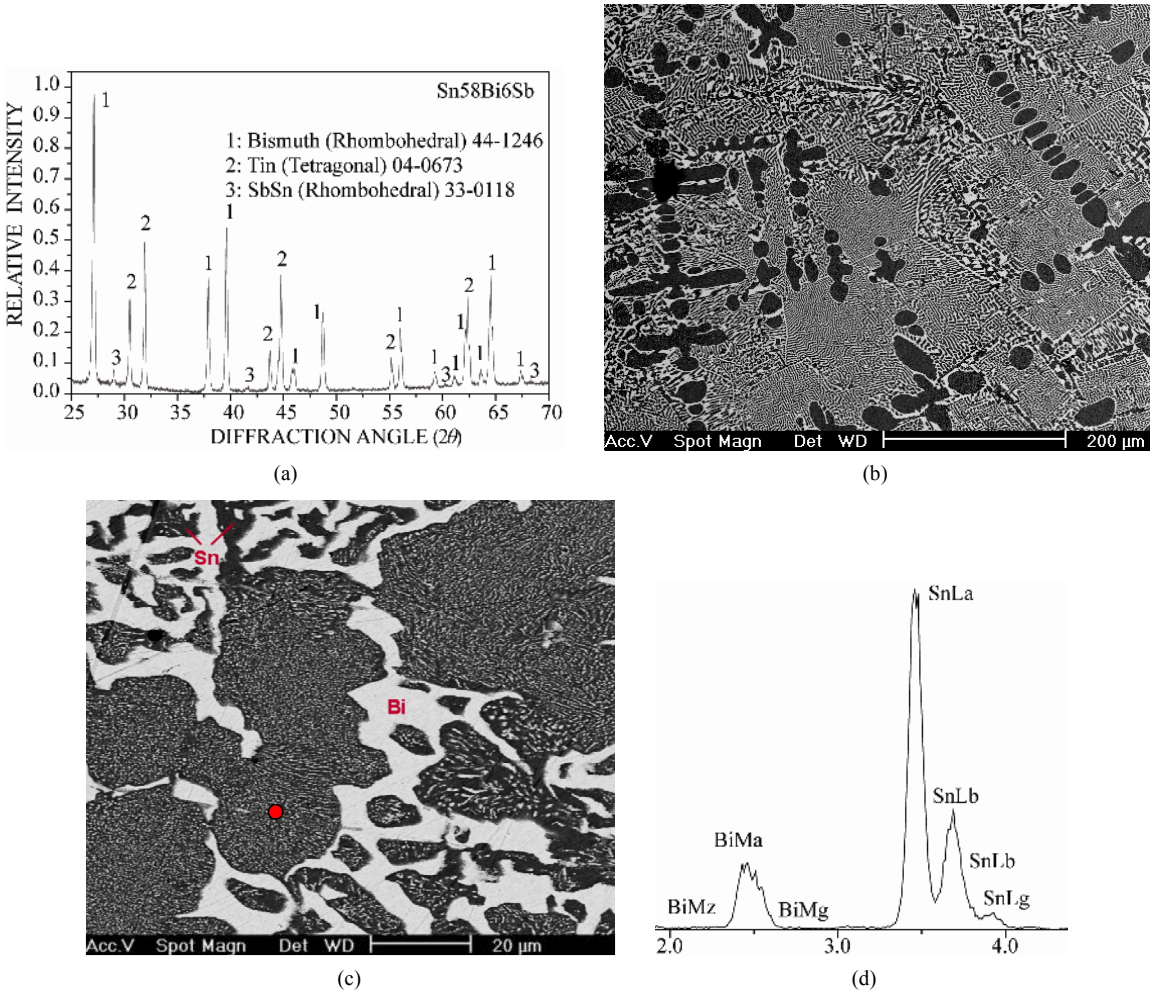

Figure 4. (a) XRD pattern obtained from the Sn-58% Bi-6% Sb alloy; (b) Image obtained by SEM from same alloy; (c) High magnification image; (d) EDX chemical analysis of the selected red zone.

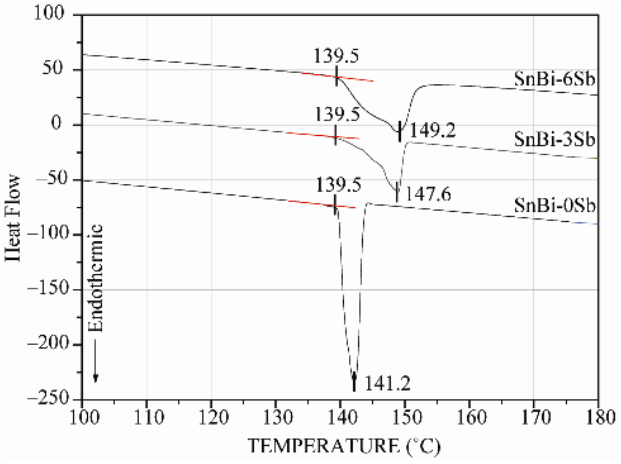

Figure 5. Thermodiagram of the as-cast manufactured solder alloys carried out in DSC at constant heating rate of 10˚C/min.

with the additions of antimony into Sn-Bi-Sb solders. It is highly preferred that the difference between solidus and liquidus temperatures of solder alloys could be reduced in order to avoid liquation during soldering [17].

For an alloy with different solidus and liquidus temperatures, the composition of the melt will gradually change as the temperature increases from the solidus to liquidus. If the portion that melts first is allowed to flow out, the remaining solid may not melt and may remain behind as a residue, which is called liquation. Alloys with narrow melting ranges do not tend to liquation, but an alloy with a wide melting range needs rapid heating cycles to minimize phase separation during soldering. It is clear that both (3 and 6 wt% Sb) additions into the Sn-Bi eutectic alloy are not still far away from the binary eutectic composition as shown in **Figure 5**. Therefore, phase separation will not become a potential problem for these solder alloys because $T_L - T_s < 10^{\circ}C$. In addition, the three alloys present a melting temperature that is smaller to the one exhibited by the eutectic alloy Sn-38Pb ($T_m = 183^{\circ}C$).

Concerning the mechanical behavior of the present

solder alloys, the homogeneous molten solder was poured into a 10 mm diameter steel tube and then cooled in the air. The rod was then machined to compressive specimens of 5 mm diameter. Specimens were not annealed to evaluate the solders. Compressive tests were carried out on the testing machine at a strain rate of 10^{-2} at 25˚C to obtain data on compressive and yielding strength, while Vickers hardness measurements were performed using 100 g before compressive testing. **Figure 6(a)** shows the compressive curve and **Figure 6(b)** the hardness behavior of the bulk solders.

As expected, it was observed the strengthening produce by the presence of the SbSn intermetallic compound. The mechanical properties of the bulk Sn-Bi-Sb solders were higher as the amount of antimony increases, making compressive strength augment from 65 MPa to almost 100 MPa when 6 wt% Sb was incorporated to the Sn-Bi alloy. Besides, hardness was increased by almost 30% as the amount of antimony augmented in the alloy. This improvement was a consequence of the detected SbSn intermetallic compound in the microstructure. Therefore, the mechanical properties of the bulk solders suggest that Sn-Bi-Sb solders have higher compressive and yielding strength as the amount of antimony increases, and hardness follows the same trend.

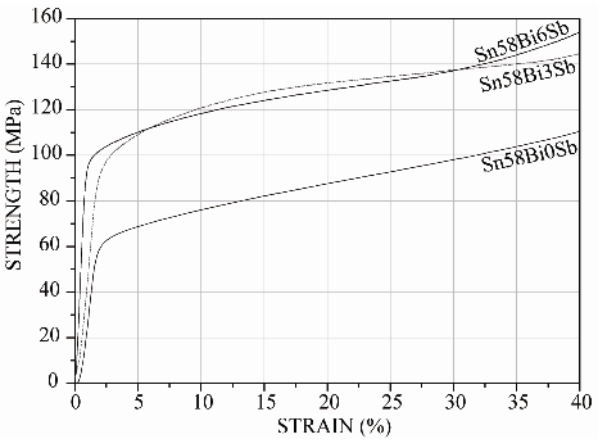

Figure 6. (a) Effect of antimony additions on stress-strain curve of Sn-Bi alloy; (b) Effect of antimony additions on hardness of Sn-Bi alloy.

In the absence of differential aeration, the formation of anodic and cathodic areas depends on the ability to ionize. Some metals ionize easily, others with difficulty and consequently anodic and cathodic areas may be produced inside the material, for example by segregation or joining of dissimilar metals. As a consequence of the microstructure observed in Sn-Bi-Sb solder alloys, anodic polarization curves were obtained for each alloy in order to evaluate the effect of Sb on the solder dissolution rate. These curves, as well as Sn-Bi-Sb alloys cathodic polarization curves and conventional Sn-38Pb alloy cathodic and anodic behavior, are showed in **Figure 7**. Cathodic and anodic curves are practically the same for the three studied alloys and they exhibit a passive behavior with a high critical current density. However, the passive area is not stable and current increases again as potential increases too. The tin-lead solder cathodic curve exhibits a smaller current density than the other alloys, while the anodic curve does not show a passivation nose as clearly as the others, although it shows a rupture potential, which exhibit very steep slopes over 1 mA/cm^2.

Table 2 shows the relevant electrochemical parameters obtained from the polarization curves of the studied alloys and compares them against the Sn-38Pb solder, composition corresponding to the Sn-Pb eutectic system composition. E_{corr} values of the studied alloys are very similar, and nobler, than the E_{corr} exhibited by the Sn-38Pb solder. A tendency toward more noble potentials is observed when increasing Sb content, which is an expected result due to the noble oxidation potentials exhibited by

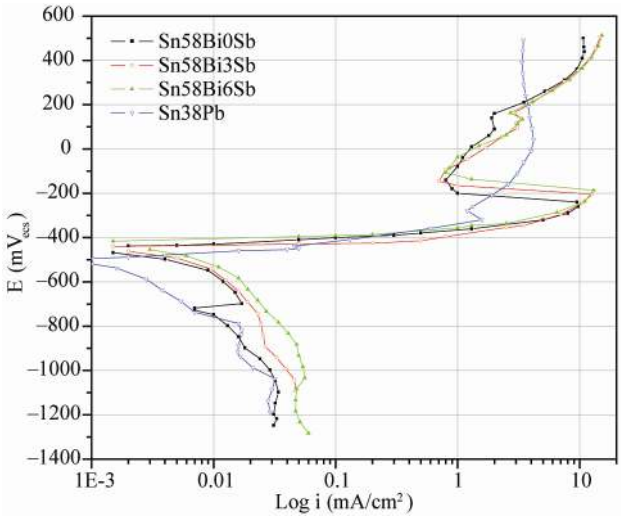

Figure 7. Typical polarization curves of SnBiSb and Sn-38Pb alloys in a 3% NaCl solution.

Table 2. Electrochemical parameters obtained from anodic polarization curves.

Alloy	E_{corr} (mV_{sce})	*Current Density*, i_{corr} (mA/cm^2)	*Passivation Current Density* (mA/cm^2)
Sn38Pb	–488	6.5×10^{-4}	4.2
Sn58Bi0Sb	–448	1.3×10^{-3}	9.7
Sn58Bi3Sb	–442	1.8×10^{-3}	12.5
Sn58Bi6Sb	–433	2.0×10^{-3}	13.0

this element [18].

The values of the corrosion current density (i_{corr}), determined by the Tafel interpolation method, are quite small and similar, even when the value corresponding to the Sn-38Pb solder is the smallest. It is observed that increasing Sb content in the SnBi alloys slightly increases i_{corr} and critical current density values. This slight increase in the i_{corr} value agrees with the statement that the behavior of lead-free solders containing antimony does not differ greatly from that of pure tin [11]. Bi and Sb are elements that exhibit nobler potentials that Sn in saline or acid solutions. However, Bi increases the preferential dissolution of Sn in acid solutions when they are alloyed [8].

4. Conclusions

It is clear that both additions into the Sn-Bi eutectic alloy, Sn-Bi-3wt%Sb (T_m = 147˚C) and Sn-Bi-6wt%Sb (T_m = 149˚C), are not still far away from the binary eutectic composition (T_m = 139˚C), therefore, liquation or phase separation will not become a potential problem for these solder alloys because $T_L - T_s < 10$˚C. In addition, these alloys present a melting temperature that is smaller to the one exhibited by the eutectic alloy Sn-38Pb (T_m = 183˚C). Moreover, the low melting temperatures of this solder alloys may permit to add more elements to further improve their properties in future works.

The mechanical properties of the bulk Sn-Bi-Sb solders were higher as the amount of antimony increases, making compressive strength increase from 65 MPa to almost 100 MPa when 6 wt% Sb was incorporated to the Sn-Bi alloy. Besides, hardness followed the same trend. This improvement was a consequence of the observed SbSn intermetallic compound in the microstructure leading to a strengthening effect.

According to these first reported electrochemical results, the addition of higher contents of Sb to the Sn-Bi eutectic alloy had opposite effects: on one hand it ennobled the E_{corr} values and on the other hand it lightly increased the i_{corr} values that are proportional to corrosion rate. Although the three studied alloys exhibited passive behavior in the solution of NaCl, their critical current density was high and the potential interval for passivity was narrow producing once again a current increase as potential was raised.

REFERENCES

[1] K. Suganuma and K. Kim, "Sn-Zn Low Temperature Solders," *Journal of Materials Science*: *Materials for Electronics*, Vol. 18, No. 1-3, 2007, pp. 121-127. doi:10.1007/s10854-006-9018-2

[2] K. N. Subramanian and J. G. Lee, "Physical Metallurgy in Lead-Free Electronic Solder Development," *JOM Journal of the Minerals*, *Metals and Materials Society*, Vol. 55, No. 5, 2003, pp. 26-32. doi:10.1007/s11837-003-0242-4

[3] J. Glazer, "Metallurgy of Low Temperature Pb-Free Solders for Electronic Assembly," *International Materials Review*, Vol. 40, No. 2, 1995, pp. 65-93. doi:10.1179/095066095790151115

[4] L. Duan, D. Q. Yu, S. Q. Han, H. T. Ma and L. Wang, "Microstructural Evolution of Sn-9Zn-3Bi Solder/Cu Joint during Long-Term Aging at 170˚C," *Journal of Alloys and Compounds*, Vol. 381, No. 1-2, 2004, pp. 202-207. doi:10.1016/j.jallcom.2004.03.124

[5] C. W. Hwang and K. Suganuma, "Joint Reliability and High Temperature Stability of Sn-Ag-Bi Lead-Free Solder with Cu and Sn-Pb/Ni/Cu Substrates," *Materials Science and Engineering*, Vol. 373, No. 1-2, 2004, pp. 187-194. doi:10.1016/j.msea.2004.01.019

[6] H. L. Lai and J. G. Duh, "Lead-Free Sn-Ag and Sn-Ag-Bi Solder Powders Prepared by Mechanical Alloying," *Journal of Electronic Materials*, Vol. 32, No. 4, 2003, pp. 215-220. doi:10.1007/s11664-003-0212-1

[7] H. W. Miao and J. G. Duh, "Microstructural Evolution in Sn-Bi and Sn-Bi-Cu Solder Joints under Thermal Aging," *Materials Chemistry and Physics*, Vol. 71, No. 3, 2001, pp. 255-271. doi:10.1016/S0254-0584(01)00298-X

[8] M. Mori, K. Miura, T. Sasaki and T. Ohtsuka, "The Corrosion of Tin Alloys in Sulfuric and Nitric Acids," *Corrosion Science*, Vol. 44, No. 4, 2002, pp. 887-898. doi:10.1016/S0010-938X(01)00094-4

[9] W. R. Osorio, L. R. Garcia, L. C. Peixoto and A. Garcia, "Electrochemical Behavior of Lead-Free Snag Solder Alloy Affected by the Microstructure," *Materials and Design*, Vol. 32, No. 10, 2011, pp. 4763-4772. doi:10.1016/j.matdes.2011.06.032

[10] D. Li, P. P. Conway and C. Liu, "Corrosion Characterization of Tin-Lead and Lead-Free Solders in 3.5 wt% NaCl Solution," *Corrosion Science*, Vol. 50, No. 4, 2008, pp. 995-1004. doi:10.1016/j.corsci.2007.11.025

[11] M. Dighe, "Corrosion of Materials," ASM International, Materials Park, 2005.

[12] H. Okamoto, "Desk Handbook: Phase Diagrams for Binary Alloys," 2nd Edition, ASM International, Materials Park, 2010.

[13] J. D. Verhoeven, "Fundamentals of Physical Metallurgy," John Wiley & Sons, New York, 1989.

[14] J. A. Dantzing and M. Rappaz, "Solidification," CRC Press, London, 2009.

[15] R. W. Cahn and P. Haasen, "Physical Metallurgy," 4th Edition, North-Holland Publishing Company, Amsterdam, 1996.

[16] W. Kurz and D. J. Fisher, "Fundamentals of Solidification," 4th Edition, Trans Tech Publications, Zurich, 1998.

[17] G. Humpston and D. M. Jacobson, "Principles of Soldering and Brazing," ASM International, Materials Park, 1993.

[18] R. Chang and J. Overby, "General Chemistry," 6th Edition, McGraw-Hill, New York, 2010.

